

Fabrication and characterization of superconducting multiqubit device with niobium base layer

Feifan Su(宿非凡), Zhaohua Yang(杨钊华), Shoukuan Zhao(赵寿宽), Haisheng Yan(严海生), Ziting Wang(王子婷), Xiaohui Song(宋小会), Ye Tian(田野), and Shiping Zhao(赵士平)

Citation: Chin. Phys. B, 2021, 30 (**10**): 100304. DOI: 10.1088/1674-1056/ac11d7
Journal homepage: http://cpb.iphy.ac.cn; http://iopscience.iop.org/cpb

What follows is a list of articles you may be interested in

Optimized pulse for stimulated Raman adiabatic passage on noisy experimental platform

Zhi-Ling Wang(王志凌), Leiyinan Liu(刘雷轶男), and Jian Cui(崔健)
Chin. Phys. B, 2021, 30 (**8**): 080305. DOI: 10.1088/1674-1056/abfccb

Quantum computation and simulation with superconducting qubits

Kaiyong He(何楷泳), Xiao Geng(耿霄), Rutian Huang(黄汝田), Jianshe Liu(刘建设), and Wei Chen(陈炜)
Chin. Phys. B, 2021, 30 (**8**): 080304. DOI: 10.1088/1674-1056/ac16cf

Fast qubit initialization in a superconducting circuit

Tianqi Huang(黄天棋), Wen Zheng(郑文), Shuqing Song(宋树清), Yuqian Dong(董煜倩), Xiaopei Yang(杨晓沛), Zhikun Han(韩志坤), Dong Lan(兰栋), and Xinsheng Tan(谭新生)
Chin. Phys. B, 2021, 30 (**7**): 070310. DOI: 10.1088/1674-1056/abff2b

Nb-based Josephson parametric amplifier for superconducting qubit measurement

Fei-Fan Su(宿非凡), Zi-Ting Wang(王子婷), Hui-Kai Xu(徐晖凯), Shou-Kuan Zhao(赵寿宽), Hai-Sheng Yan(严海生), Zhao-Hua Yang(杨钊华), Ye Tian(田野), Shi-Ping Zhao(赵士平)
Chin. Phys. B, 2019, 28 (**11**): 110303. DOI: 10.1088/1674-1056/ab4578

Demonstration of quantum permutation parity determine algorithm in a superconducting qutrit

Kunzhe Dai(戴坤哲), Peng Zhao(赵鹏), Mengmeng Li(李蒙蒙), Xinsheng Tan(谭新生), Haifeng Yu(于海峰), Yang Yu(于扬)
Chin. Phys. B, 2018, 27 (**6**): 060305. DOI: 10.1088/1674-1056/27/6/060305

Fabrication and characterization of superconducting multiqubit device with niobium base layer*

Feifan Su(宿非凡)[1], Zhaohua Yang(杨钊华)[1,2], Shoukuan Zhao(赵寿宽)[1,2], Haisheng Yan(严海生)[1,2], Ziting Wang(王子婷)[1,2], Xiaohui Song(宋小会)[1], Ye Tian(田野)[1], and Shiping Zhao(赵士平)[1,2,3,4,†]

[1] *Beijing National Laboratory for Condensed Matter Physics, Institute of Physics, Chinese Academy of Sciences, Beijing* 100190, *China*
[2] *School of Physical Sciences, University of Chinese Academy of Sciences, Beijing* 100190, *China*
[3] *Chinese Academy of Sciences Center for Excellence in Topological Quantum Computation, University of Chinese Academy of Sciences, Beijing* 100190, *China*
[4] *Songshan Lake Materials Laboratory, Dongguan* 523808, *China*

(Received 25 February 2021; revised manuscript received 2 July 2021; accepted manuscript online 7 July 2021)

Superconducting transmon qubits are the leading platform in solid-state quantum computing and quantum simulation applications. In this work, we develop a fabrication process for the transmon multiqubit device with a niobium base layer, shadow-evaporated Josephson junctions, and airbridges across the qubit control lines to suppress crosstalk. Our results show that these multiqubit devices have well-characterized readout resonators, and that the energy relaxation and Ramsey (spin-echo) dephasing times are up to ~ 40 μs and 14 (47) μs, respectively. We perform single-qubit gate operations that demonstrate a maximum gate fidelity of 99.97%. In addition, two-qubit vacuum Rabi oscillations are measured to evaluate the coupling strength between qubits, and the crosstalk among qubits is found to be less than 1% with the fabricated airbridges. Further improvements in qubit coherence performance using this fabrication process are also discussed.

Keywords: superconducting quantum computing, transmon qubit, device fabrication, characterization

PACS: 03.67.Lx, 03.65.Yz, 85.25.Cp, 74.50.+r **DOI:** 10.1088/1674-1056/ac11d7

1. Introduction

Superconducting circuits based on circuit quantum electrodynamics (cQED) have become a strong competitor in solid-state quantum computing and a convenient platform for quantum simulation.[1–8] In the circuit commonly known as the transmon qubit, the manipulation and readout of the quantum state are accomplished by control lines and mediated by qubit dispersive coupling to a transmission-line resonator.[9–11] Transmon qubits have proved favourable in several respects, such as quantum coherence time, device scalability, quantum-state manipulation, and fast state readout. The device fabrication process is also relatively simple (compared to the case of phase qubits, for example), which, in the planar single-chip case, usually consists of a large-area base layer, shadow-evaporated Josephson junctions, and airbridges used to reduce qubit crosstalk.[12] At present, superconducting transmon qubits with aluminum (Al) base layers are used in many studies, while some research groups are studying and looking for new materials for qubit devices, such as niobium (Nb) and tantalum (Ta).[13–15]

Using Nb base layers for the transmon qubits may offer advantages in terms of device fabrication, circuit wiring, and scaling up for more qubits. Nb films, for instance, have less electron-beam transparency than Al films, and the patterning can easily be positioned using the e-beam lithographic process (a gold mark layer is often prepared in Al-based devices).[16] The dry etching process of the Nb film is also relatively simple and stable. In addition, Nb is a hard metal, which does not react with the resist developer, and allows repeated wire bonding and room-temperature resistance measurements of the Josephson junctions using a four-point needle apparatus. Finally, it could be convenient for the scaling up for more qubit, using techniques such as 3D flip-chip wiring,[17] since interdiffusion with the indium layer will not occur, and an additional layer of TiN is not required in the 3D packaging process.

In this work, we present a detailed description of the fabrication of the superconducting transmon multiqubit device with Nb base layer. The fabrication process starts with a substrate treatment that does not involve cleaning in solvents such as piranha solution and ends with a special photoresist removal procedure following airbridge preparation. Our preliminary results show that the resulting qubit devices have energy relaxation and Ramsey (spin-echo) dephasing times as high as ~ 40 μs and 14 (47) μs, respectively. Single-qubit gate operations are performed, and demonstrate a maximum gate fidelity of 99.97%. Two-qubit vacuum Rabi oscillations are also measured to evaluate the coupling strength between qubits, and the

*Project supported by the National Key R&D Program of China (Grant No. 2016YFA0300601), the National Natural Science Foundation of China (Grant Nos. 11934018 and 11874063), the Strategic Priority Research Program of the Chinese Academy of Sciences (Grant No. XDB28000000), and the Key-Area Research and Development Program of GuangDong Province, China (Grant No. 2018B030326001).

†Corresponding author. E-mail: spzhao@iphy.ac.cn

© 2021 Chinese Physical Society and IOP Publishing Ltd

crosstalk among qubits is found to be less than 1% due to the use of airbridges across the qubit control lines. These results indicate that Nb-based qubits with excellent properties can be prepared using this simple fabrication process. Further improvements related to the qubit coherence properties, etc. can be expected and will be briefly discussed.

2. Sample fabrication

Figure 1(a) shows an optical micrograph of the central part of the superconducting ten-qubit device fabricated in this study using a Nb base layer. Each qubit is coupled to a $\lambda/4$ readout resonator, which is, in turn, coupled to a transmission line for measurement. In Fig. 1(b), the enlargement shows the qubit's SQUID loop, in which the microwave line for XY control and the flux bias line for Z control can clearly be seen (the second, fourth, seventh, and ninth qubits do not have a separate XY line in this design). An airbridge across a microwave excitation line is shown in Fig. 1(c). The ten-qubit device is designed to have a central readout resonator frequency of 6.35 GHz with a separation of about 12.5 MHz between neighboring resonators. The qubit–resonator coupling strength is about 30 MHz and the qubit–qubit coupling strength is 10–20 MHz. The designed qubit frequency is 5.0 GHz.

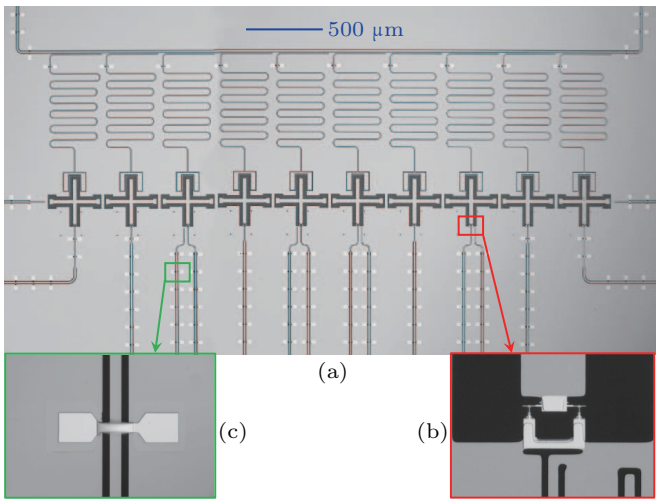


Fig. 1. Microscope images of (a) the central region of the fabricated coupled 10-qubit device, (b) the SQUID loop area containing two Josephson junctions, and (c) an airbridge across the control line.

As can be seen in Fig. 1, the superconducting ten-qubit device is made up of four film layers: the Nb base layer (light grey areas), the double Al layers made by shadow evaporation forming Josephson junctions [white area in Fig. 1(b)], and the Al layer of airbridges [white small bridges in Figs. 1(a) and 1(c)]. The fabrication process started with the DC-sputter deposition of a 100 nm-thick Nb film at room temperature on a two-inch, 430-μm-thick sapphire substrate, which was plasma cleaned in a mixture of oxygen and argon gases, and heat treated at 350 °C for two hours in a load lock chamber before sputtering. Sputtering was performed in an ultrahigh vacuum system with a background pressure of 8×10^{-8} Pa, at an Ar working pressure of 1.7 Pa with a deposition rate of 1.05 nm/s. X-ray diffraction and electrical measurements revealed a film lattice constant of 0.3303 nm (close to the bulk value), a superconducting transition temperature of 9.1 K, and a residual resistivity ratio (RRR) between 4 and 7. It was found that the RRR increased with increasing substrate temperatures during sputter deposition.

The film was spin-coated with S1813 photoresist at 500 rpm for 5 s and then at 4000 rpm for 60 s, resulting in a 1.3 μm thick photoresist layer, which was subsequently solidified at 115 °C for 1 min. The photolithographic patterning was performed using a DWL66+ laser direct-writing system with a laser writing head with a 4 mm aperture. The photoresist layer was developed in ZX-238 developer for 40 s at a constant temperature of 25 °C and fixed in deionized water for 30 s. The sample was subsequently dry etched in a Samco 10NR reactive-ion etching system using SF_6 at a pressure of 4.5 Pa with a flow rate of 50 sccm and a power of 50 W for 3 min. During the etching process, we found it crucial to keep the reflection power as low as possible, since it is directly related to photoresist edge deterioration. A reflection power close to zero leads to high-fidelity image transfer and an unevenness of the final patterned edges of the Nb film structures on the order of 30 nm or less.

The next step was to prepare the MAA/PMMA double layer for the shadow evaporation of the Josephson junctions. Consequently, the sample was first spin-coated with a 200 nm-thick MAA 11 layer at 500 rpm for 5 s and then at 5000 rpm for 60 s, and baked at 170 °C for 2 min. A 300-nm thick PMMA 950 layer was then coated and baked at 170 °C for 15 min. The double-layer resist was e-beam exposed in a 20 keV Raith 150 system with a step size of 20 nm and an aperture diameter of 20 μm using areal doses of 200 μC/cm^2 and 45 μC/cm^2, respectively. The sample was subsequently developed in MIBK:IPA (1:3) developer at 25 °C for 50 s and fixed for 10 s in deionized water.

The shadow evaporation of the Josephson junctions for the qubit device was carried out in a JEB4 system, a four-chamber ultrahigh-vacuum system with electron-beam evaporation, ion-milling, oxidation, and load lock capabilities. Precleaning in Ar gas was first performed to remove the impurities and nonconducting layers from the Nb film surface so that the Al junction electrodes could form superconducting connections with the Nb film. The thicknesses of the bottom and top Al electrodes were 65 nm and 100 nm, and angles of $-62°$ and $0°$ were used for the evaporation, respectively. An oxidation time of 57 minutes and an oxygen pressure 3.6 Torr were used for the tunnel barrier formation, which led to a junction critical current density J_c of 60 A/cm^2. The sample was then soaked in an NMP solution at a fixed temperature of 40 °C for

two hours and finally lifted off.

The final step was to prepare airbridges across the device control lines in order to suppress crosstalk among qubits, which is necessary for precise multiqubit manipulation and operation.[18–22] To do so, we prepared a SPR220 resist layer and used laser direct writing for the patterning; the 300-nm thick Al film bridges were fabricated by electron beam evaporation and subsequent lift off. The time spent in Ar ion milling before evaporation has to be carefully determined in the preparation process. When the time is too short, the superconducting connection between the airbridges and the bottom Nb film is insufficient. On the other hand, if the time is too long, the lift off process and residual resist removal become difficult. In this work, Ar ion milling was performed with an RF power of 170 W for 90 s. A resist removal process using specially designed apparatus was employed for this experiment.[23]

3. Sample characterization and discussion

We present and discuss the experimental results for three samples fabricated using the above process.[24] In the cQED architecture, the qubit state is probed by the so-called dispersive readout technique.[9,10] In brief, when the qubit is detuned from the resonator frequency, it induces a state-dependent frequency shift of the resonator from which the qubit state can be inferred. Hence, the readout fidelity of the qubit state depends critically on the resonator property, which is related to the quality factor Q and the ω_r of the resonator. The measurement can be performed by sending a signal V_{in} into one end of the transmission line and detecting the output signal V_{out} at the other. The transmission coefficient $S_{21} = V_{out}/V_{in}$ can be written as $S_{21}^{-1}(\omega) = 1 + e^{i\varphi}(Q_i/Q_c)[1/(1 + 2iQ_i(\omega - \omega_r)/\omega_r)]$, where Q_i and Q_c are the internal and coupling quality factors, respectively, and φ is the phase difference caused by the input and output impedance mismatch.[25] In this work, the average values of the internal quality factor and the coupling quality factor were found to be $Q_i = 281935$ and $Q_c = 10254$ by fitting the experimental S_{21} data. The total or loaded quality factor Q_l, defined by $Q_l^{-1} = Q_i^{-1} + Q_c^{-1}$, is therefore approximately 9898.

The qubit coherence times, including the energy relaxation and dephasing times, which can be measured in separate experiments,[4,5,26,27] are listed in Table 1 for samples I and II. With known resonator responses to the qubit ground and first excited states, the energy spectra of each qubit can be measured by varying the flux bias through the Z control lines. Rabi oscillations are then measured by turning on a microwave pulse that is resonant with the qubit frequency for a given time τ and measuring the first excited state population (probability P_1) after a short delay. The π-pulse amplitude and length are obtained from the $P_1 \sim \tau$ dependence, which can be used to excite the qubit from the ground state to the excited state. In Fig. 2, we show the experimental energy relaxation characteristic and the fitted relaxation time of $T_1 = 31.4$ μs for qubit nine of sample II. The data were obtained by initializing the qubit in the ground state, applying a π pulse for the excitation to the excited state, waiting for a given period of time τ, and measuring the probability P_1. By changing the qubit flux bias and repeating the above process, we obtained the energy relaxation time T_1 for different qubits and frequencies and its variation with time. The average relaxation time was found to be 26.9 μs for this qubit and the longest time was up to 40 μs. The variations of T_1 with frequency and time are shown in the inset of Fig. 2.

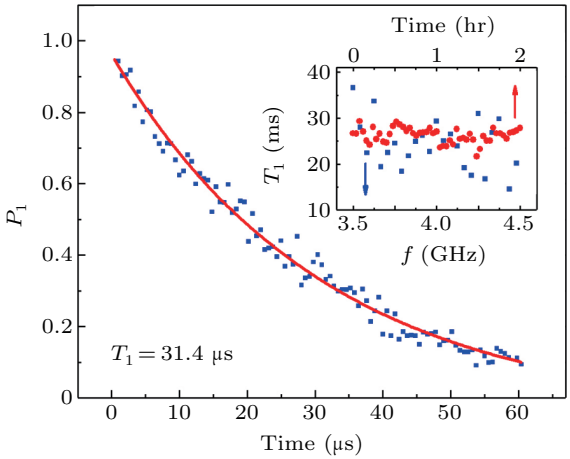


Fig. 2. Experimental (symbols) and fitted (line) results of the energy relaxation process for qubit nine of sample II. The inset shows the variations of T_1 with qubit frequency (squares) and time (circles).

Table 1. Energy relaxation time T_1, Ramsey and spin-echo dephasing times T_φ and T_{2E}, measured near the qubit maximum frequency f_{01} for sample I. Data in parentheses are from sample II.

Qubit	Q_1	Q_2	Q_3	Q_4	Q_5	Q_6	Q_7	Q_8	Q_9	Q_{10}
f_{01} (GHz)	4.892	4.847	4.967	5.004	5.037	5.116	5.046	4.979	4.911 (4.643)	5.038
T_1 (μs)	26.9	19.1	17.5	18.6	17.6	24.9	26.8	18.5	25.1 (26.9)	24.7
T_φ (μs)	4.755	2.336	6.581	3.913	3.001	9.249	4.419	8.117	1.821 (14.1)	3.063
T_{2E} (μs)	15.73	11.39	15.668	10.4	15.879	21.94	47.1	27.93	7.298 (27.5)	18.367

The qubit dephasing time can be determined from the Ramsey interference experiment, which measures the non-driven, freely precessing qubit state.[27] In this experiment a $\pi/2$ microwave pulse around the x-axis tips the state vector from the north pole down to the equator, which is allowed to rotate in the x–y plane for a given time τ before being projected back by a second $\pi/2$ pulse. Furthermore, when a π pulse around the x-axis is inserted between the two $\pi/2$ pulses in

the Ramsey experiment, a spin-echo experiment is performed, which removes the line-broadening associated with the low-frequency noise of the qubit precession, and allows the observation of improved qubit coherence after the low-frequency dephasing noise has been mitigated. The measured dephasing time and characteristic time of the spin-echo experiment were up to $T_\varphi = 14.1$ μs and $T_{2E} = 47.1$ μs, respectively. The typical measured values together with T_1 are listed in Table 1 for all qubits of sample I and qubit nine of sample II.

We characterize the single qubit gate fidelity by the randomized benchmarking method.[28,29] In this method, the qubit is first prepared in the ground state and a sequence of m Clifford gates are randomly chosen to drive the qubit. The m Clifford gates are either applied successively or interleaved with a specific gate H. The measurement of the remaining population of the initial state after the gate operations gives rise to the reference and gate sequence fidelities F, respectively, which can be fitted using $F = Ap^m + B$, where A and B are constants and p is a depolarizing parameter. In Fig. 3, we show the results for $H = Y_{-\pi/2}$ measured for qubit eight of sample I. For each sequence length m, we repeat the measurement 30 times (the open symbols represent their average values). By fitting to these values as a function of m, we obtain the parameters $p_{\rm ref}$ and $p_{\rm gate}$. The gate fidelity is then calculated by $F_{\rm gate} = 1 - (1 - p_{\rm gate}/p_{\rm ref})/2$ to be 99.86%. In Table 2, we list the experimental results for several other gate operations with fidelities as high as 99.97% in the case of $H = X_{\pi/2}$.

Table 2. Gate fidelities measured at $f = 4.979$ GHz for qubit eight of sample I.

Gate	X	$X_{\pi/2}$	$X_{-\pi/2}$	Y	$Y_{\pi/2}$	$Y_{-\pi/2}$
Fidelity (%)	99.88	99.97	99.92	99.94	99.91	99.86

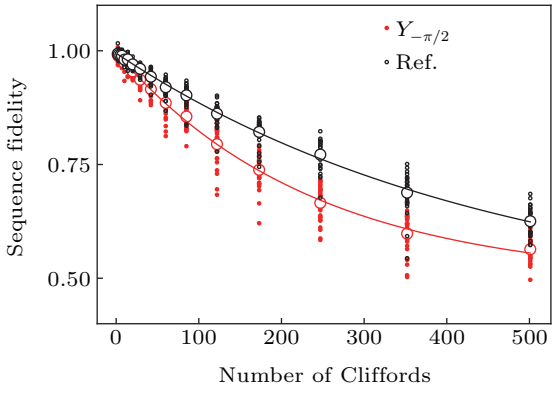


Fig. 3. Sequence fidelities as a function of the number of Clifford gates in a randomized benchmarking experiment for qubit eight of sample I. See text for further details.

Two-qubit vacuum Rabi oscillations are useful for the evaluation of the qubit coupling strength as well as calibrations of the Z-pulse amplitude and the iSWAP gate operation parameters.[30] Figure 4 shows the result when the frequency of qubit seven of sample I is fixed at 4.568 GHz and a Z-pulse with a changing amplitude is applied to qubit eight to vary its frequency near the resonant point with qubit seven. Qubits seven and eight are prepared in the ground and first excited states, respectively, and for each Z-pulse amplitude, the excited-state populations of both qubits are measured as a function of time. In Fig. 4, we can see a clear excitation swap between the two qubits. At the central frequency, the fitted maximum period is 23.88 ns (or a minimum frequency of 41.88 MHz), which corresponds to a qubit–qubit coupling strength of 20.9 MHz.

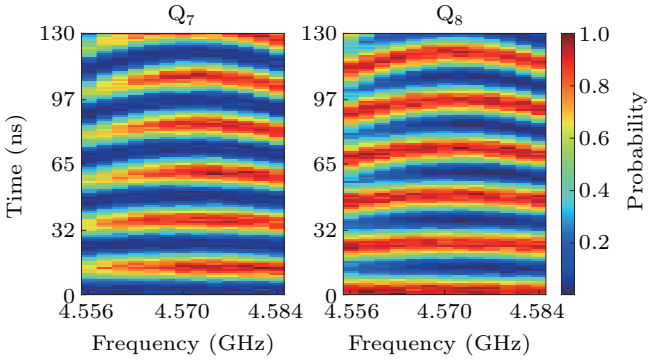


Fig. 4. Vacuum Rabi oscillation between qubits seven and eight of sample I.

For multiqubit devices and experiments, the crosstalk among qubits, i.e., the case in which one qubit is manipulated via the Z and/or XY control lines and other qubits also experience the change, is notorious, and greatly hinders qubit manipulation.[17,31,32] In this work, we fabricated Al airbridges across the control lines (see Fig. 1) to overcome this problem. Since a change of qubit frequency causes the resonator frequency to change, one can detect the crosstalk among qubits, for example, by varying the flux bias of one qubit and monitoring the resonator frequency changes of the other qubits. Figure 5 shows the results for sample III. When we change the flux bias of qubit eight, its resonator frequency shows periodic changes (middle panel) as expected, while the corresponding changes in the neighbouring qubits, seven and nine, can hardly be seen (left and right panels). A detailed analysis of the Z-pulse crosstalk matrix measurements indicates that the crosstalk among qubits is less than 1%.

Our results demonstrate that transom qubit devices with Nb films as their base electrodes fabricated using the simple fabrication process described above can have excellent properties and performance. We note that the experimentally determined device parameters, including the resonator frequencies, qubit-resonator coupling strength, qubit frequencies, as well as the qubit–qubit coupling strength measured by SWAP spectroscopy, are close to the designed values. The qubit coherence times are comparable to the results recently reported by the Princeton group using similar preparation conditions, which included an energy relaxation time of $T_1 = 23$ μs.[33] Further improvements in the device coherence properties could be expected if more sophisticated substrate cleaning procedures and elevated substrate temperatures were used during the growth

of the Nb film.[22,34–36] In addition, further optimizations of the device design and the use of alternative materials could improve the qubit performance beyond the limitations of the device fabrication process.[32,33,37–39]

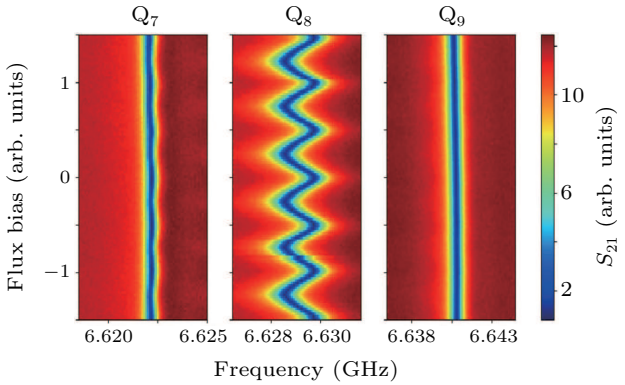


Fig. 5. Changes of the resonator frequencies from qubit seven to qubit nine of sample III (left to right panels) when only qubit eight is subjected to a changing flux bias, showing an extremely small crosstalk among qubits.

4. Summary

We have developed a fabrication process for superconducting transmon multiqubit devices with Nb base layers, shadow evaporated Josephson junctions, and airbridges for suppressing crosstalk among qubits. The fabricated multiqubit devices demonstrated excellent coherence properties, high gate fidelities, and small crosstalk. Two-qubit vacuum Rabi oscillations were measured to evaluate the qubit–qubit coupling strength. Our work provides a simple and convenient fabrication process, which could be useful for scaling up to more qubits, or the use of similar hard metal materials, such as Ta, for qubit fabrication. Further improvements in qubit coherence properties using these materials should be possible by modifying the substrate treatment and surface cleaning process, as well as by elevating the substrate temperature during film deposition.

Acknowledgment

We are grateful to the Laboratory of Microfabrication at the Institute of Physics for technical help.

References

[1] Arute F, Arya K, Babbush R, Bacon D, Bardin J C, Barends R, Biswas R, Boixo S, Brandao F G S L and Martinis J M 2019 *Nature* **574** 505
[2] Krantz P, Kjaergaard M, Yan F, Orlando T P, Gustavsson S and Oliver W D 2019 *Appl. Phys. Rev.* **6** 021318
[3] Devoret M H and Schoelkopf R J 2013 *Science* **339** 1169
[4] Wendin G and Shumeiko V S 2006 *Handbook of Theoretical and Computational Nanotechnology* (Rieth M and Schommers W, Ed.) (California: American Scientific Publishers)
[5] Clarke J and Wilhelm F K 2008 *Nature* **453** 1031
[6] Makhlin Y, Schon G and Shnirman A 2001 *Rev. Mod. Phys.* **73** 357
[7] Georgescu I M, Ashhab S and Nori F 2014 *Rev. Mod. Phys.* **86** 153
[8] Cirac J I and Zoller P 2012 *Nat. Phys.* **8** 264
[9] Blais A, Huang R, Wallraff A, Girvin S M and Schoelkopf R J 2004 *Phys. Rev. A* **69** 062320
[10] Koch J, Yu T, Gambetta J, Houck A A, Schuster D I, Majer J, Blais A, Devoret M H, Girvin S M and Schoelkopf R J 2007 *Phys. Rev. A* **76** 042319
[11] Liu W Y, Zheng D N and Zhao S P 2018 *Chin. Phys. B* **27** 027401
[12] Josephine B C, Michael R V, Antonio D C, Martin S, Gao J, David W A, Jerry M C, Jay M G, Mary B R, George A K, Matthias S and David P P 2011 *Appl. Phys. Lett.* **103** 012602
[13] Calusine G, Melville A, Woods W, Das R, Stull C, Bolkhovsky V, Braje D, Hover D, Kim D K, Miloshi X, Rosenberg D, Sevi A, Yoder J L, Dauler E and Oliver W D 2018 *Appl. Phys. Lett.* **112** 062601
[14] Liu Q, Xue G M, Tan X S, Yu H F and Yu Y 2017 *Chin. Phys. B* **26** 058402
[15] Foxen B 2018 *Quantum. Sci. Technol.* **3** 014005
[16] Su F F, Wang Z T, Xu H K, Zhao S K, Yan H S, Yang Z H, Tian Ye and Zhao S P 2019 *Chin. Phys. B* **28** 110303
[17] Chen Z, Megrant A, Kelly J, Barends R, Bochmann J, Chen Yu, Chiar B, Dunsworth A, Jeffrey E, Mutus J Y, Malley P J J, Neill C, Roushan P, Sank D, Vainsencher A, Wenner J, White T C, Cleland A N and Martinis J M 2014 *Appl. Phys. Lett.* **104** 052602
[18] Jin Z C, Wu H T, Yu H F and Yu Y 2018 *Chin. Phys. B* **27** 100310
[19] Ponchak G E, Papapolymerou J and Tentzeris M M 2005 *IEEE Trans. Microwave Theory Techniq.* **53** 713
[20] Liaw H J and Merkelo H 1997 *IEEE Circ. Dev. Mag.* **13** 22
[21] Schuster C and Fichtner W 2001 *IEEE Trans. Electromagn. Compat.* **43** 416
[22] Megrant A, Neill C, Barends R, Chiaro B, Chen Yu, Feigl L, Kelly J, Lucero E, Mariantoni M, Malley P J J, Sank D, Vainsencher A, Wenner J, White T C, Yin Y, Zhao J, Palmstrm C J, Martinis J M and Cleland A N 2012 *Appl. Phys. Lett.* **100** 113510
[23] Su F F, Yang Z H, Tian Y and Zhao S P *Chinese Invention Patent* 2020110193710.0 [2021-04-15] (in Chinese)
[24] Airbridges are fabricated on sample III, which does not show difference compared to samples I and II in the coherence time measurements.
[25] Suri B 2015 *Transmon qubits coupled to superconducting lumped element resonators* (University of California, Santa Barbara)
[26] Bylander J, Gustavsson S, Yan F, Yoshihara F, Harrabi K, Fitch G, Cory D G, Nakamura Y, Tsai J S and Oliver W D 2011 *Nat. Phys.* **7** 565
[27] Mao B 2010 *Coherent Manipulation of Multi-Partite Quantum States in a Qubit-TLS System via Landau-Zener Transition* (Ph.D Dissertation) (Lawrence: University of Kansas)
[28] Chow J M, Gambetta J M, Tornberg L, Koch J, Bishop L S, Houck A A, Johnson B R, Frunzio L, Girvin S M and Schoelkopf R J 2009 *Phys. Rev. Lett.* **102** 090502
[29] Magesan E, Gambetta J M and Emerson J 2011 *Phys. Rev. Lett.* **106** 180504
[30] Steffen M, Ansmann M, Bialczak R C, Katz N, Lucero E, McDermott R, Neeley M, Weig E M, Cleland A N and Martinis J M 2006 *Science* **313** 1423
[31] Majer J, Chow J M, Gambetta J M, Koch J, Johnson B R, Schreier J A, Frunzio L, Schuster D I, Houck A A, Wallraff A, Blais A, Devoret M H, Girvin S M and Schoelkopf R J 2007 *Nature* **449** 443
[32] Houck A A, Schreier J A, Johnson B R, Chow J M, Koch J, Gambetta J M, Schuster D I, Frunzio L, Devoret M H, Girvin S M and Schoelkopf R J 2008 *Phys. Rev. Lett.* **101** 080502
[33] Place P M, Rodgers V H, Mundada P, Smitham M, Fitzpatrick M, Leng Z Q, Premkumar A, Bryon J, Sussman S, Cheng G M, Madhavan T, Babla H K, Jack B, Gyenis A, Yao N, Cava R J and Houck A A 2020 arXiv:2003.00024v1 [quant-ph]
[34] Gambetta J M, Murray C E, Fung Y K K, McClure D T, Dial O, Shanks W, Sleight J and Steffen M 2017 *IEEE Trans. Appl. Supercond.* **27** 1
[35] Wang H, Hofheinz M, Wenner J, Ansmann M, Bialczak R C, Lenander M, Lucero Erik, Neeley M, Connell A D, Sank D, Weides M, Cleland A N and Martinis J M 2009 *Appl. Phys. Lett.* **95** 233508
[36] Blok M S, Ramasesh V V, Schuster T, Brien K, Kreikebaum J M, Dahlen D, Morvan A, Yoshida B, Yao N and Siddiqi I 2020 arXiv:2003.03307v1 [quant-ph]
[37] Geerlings K, Shankar S, Edwards E, Frunzio L, Schoelkopf R J and Devoret M H 2012 *Appl. Phys. Lett.* **100** 192601
[38] Sage J M, Bolkhovsky V, Oliver W D, Turek B and Welander P B 2011 *J. Appl. Phys.* **109** 063915
[39] Bilmes A, Neumann A K, Volosheniuk S, Ustinov A V and Lisenfeld J 2021 arXiv:2101.01453v2 [quant-ph]